Supporting Information

Mass Action at the Single-Molecule Level

Min Ju Shon and Adam E. Cohen*
*cohen@chemistry.harvard.edu
Departments of Chemistry and Chemical Biology and of Physics, Harvard University, Cambridge, Massachusetts 02138, United States

Table of Contents

Part I. Construction of the Dimple Machine

Figure S1. Nanofabrication of dimple arrays

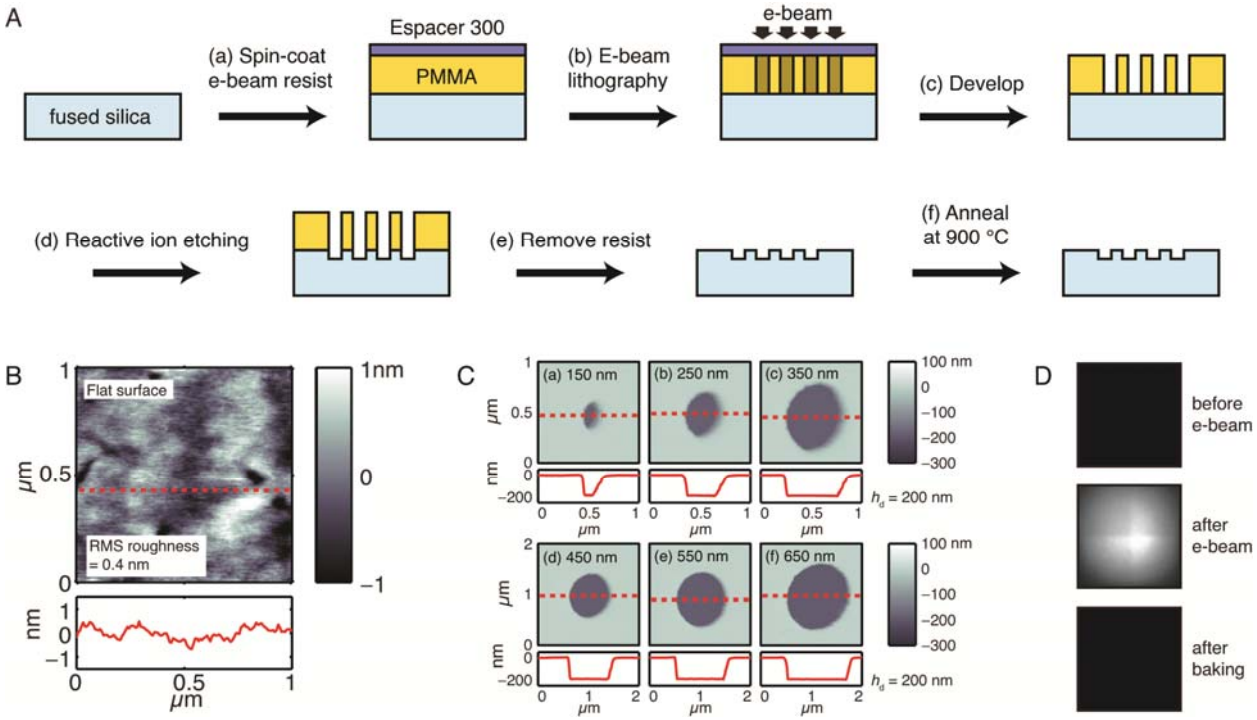

(A) Scheme for the nanofabrication. (a) A 1" square fused silica coverslip (Esco, R425025 S1-UV) was cleaned in piranha solution (3:1 sulfuric acid : hydrogen peroxide) at 70 °C for 30 min, followed by rinsing in water. The substrate was then spin-coated with adhesion promoter (ShinEtsu, MicroSi MicroPrime HP Primer, at 1,000 rpm), electron-beam lithography resist poly(methyl methacrylate) (PMMA, MicroChem, 950 A4, at 3,000 rpm), and conducting polymer (electron-discharge layer, Showa Denko, Espacer300, at 1,000 rpm). (b) Electron-beam lithography was carried out by JEOL JSM-7000F at an accelerating voltage of 30 kV and an electron dose in the range of 700–1,200 μC/cm^2. Typically 40 dimple arrays were written on one substrate during the exposure, and each array (120 μm × 120 μm) contained 900 circular dimples of varying sizes, arranged in a square lattice with spacing 4 μm. (c) The processed substrate was (1) washed in water to dissolve the conducting polymer layer, (2) developed in 1:3 methyl isobutyl ketone : isopropyl alcohol (IPA) for 2 min, and (3) washed in IPA. (d) The developed substrate was briefly cleaned by oxygen plasma (Technics Micro-stripper, 30 mTorr of oxygen for 30 s) and the exposed fused silica was etched in a reactive ion etching system (STS-ICP-RIE) by fluorine-based recipe using PMMA as an etch mask. (e) PMMA after etching was completely removed by dissolving in acetone and in 2 % Hellmanex solution in

water at 70 °C for 30 min. (f) The nanofabricated fused silica was annealed in a furnace at 900 °C for 5 h to remove the autofluorescence from the fused silica induced by the e-beam lithography (Section S2).

(B) Clean surface of a fused silica coverslip. (*top*) Atomic microscope (AFM, Asylum Research, MFP-3D) image of the surface of a fused silica coverslip after cleaned in piranha solution. Root-mean-square surface roughness was 0.4 nm. (*bottom*) Section of the image along the red line in (top).

(C) Nanofabricated dimples on a fused silica coverslip. (*top*) Images of the dimples with nominal radii of (a) 150, (b) 250, (c) 350, (d) 450, (e) 550, (f) 650 nm. (*bottom*) Section of the scan along the red dashed line in the (top) image. The final depth of etching was measured to be 190–200 nm for all dimples.

(D) Autofluorescence of the fused silica. Surface of a fused silica coverslip imaged on a fluorescence microscope exciting at 633 nm. All images are displayed with the same brightness and contrast. (*top*) Initial autofluorescence was sufficiently low to allow detection of single-molecules. (*middle*) Electron-beam lithography led to an increase in autofluorescence by > 1000-fold, in an electron-dose-dependent manner (Section S2). (*bottom*) Baking the finished fused silica wafer in a furnace at 900 °C for 5 h completely eliminated the electron beam-induced fluorescence (Section S2), without distorting the nanofabricated dimples.

Figure S2. Microfabrication of the lid with microposts

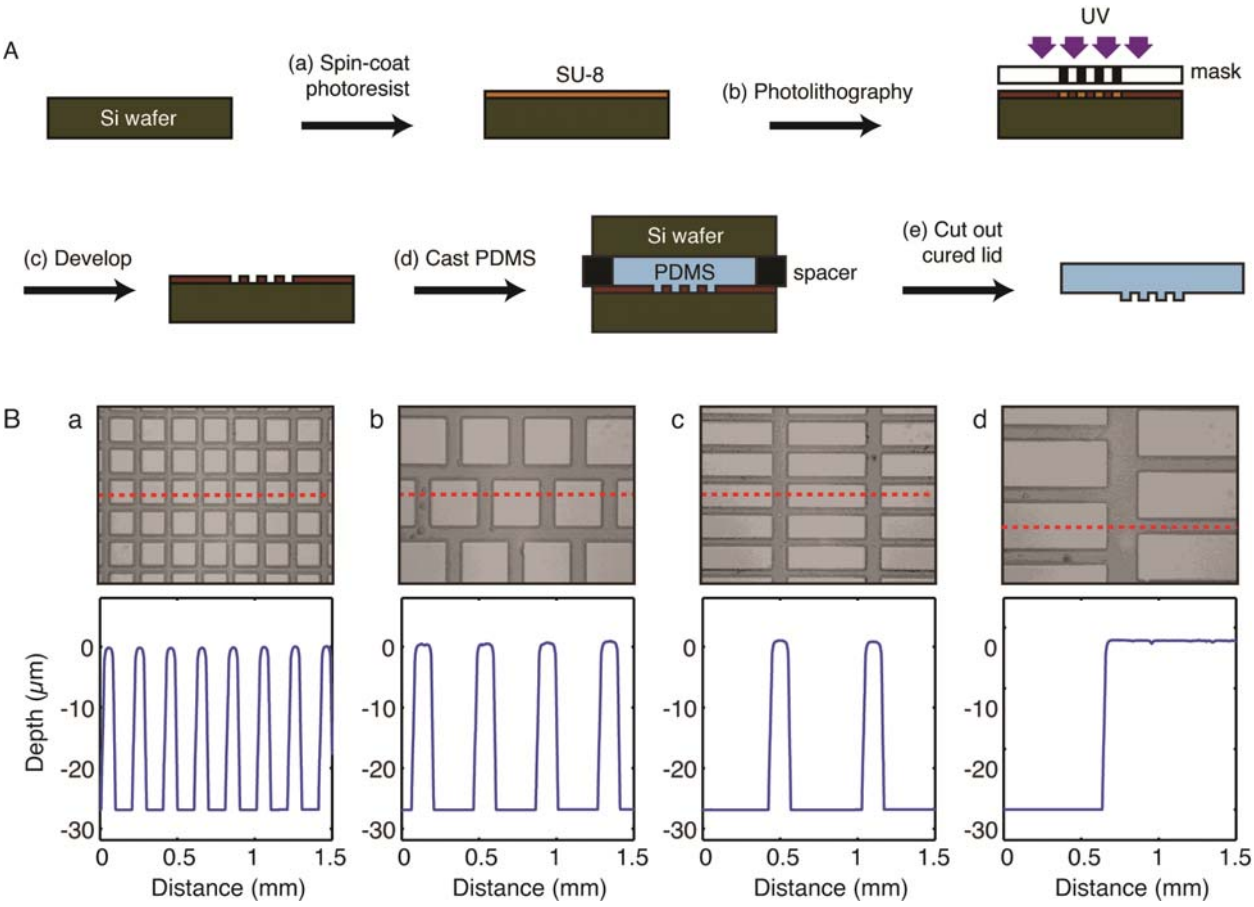

(A) Scheme for the Microfabrication of the lid. (a) A 3" silicon wafer was cleaned by sonicating in acetone, IPA, and methanol, successively, for 5 min each, rinsed in water, and dried on a hotplate. The cleaned wafer was coated with a negative photoresist SU-8 (MicroChem, SU-8 3025) and baked on a hotplate at 95 °C for 15 min. (b) The cured resist was exposed through a transparency mask to UV for 15 min. The substrate was baked on a hotplate at 65–95 °C for 5 min. (c) The resist was developed in SU-8 developer (MicroChem) for 10 min. The wafer was thoroughly rinsed with IPA and hard-baked at 200 °C for 30 min. (d) The fabricated SU-8 microstructures served as a master for the fabrication of the PDMS lid. Two-part mixture of PDMS (Dow Corning, Sylgard 184, 10:1 base : curing agent) was poured over the master and topped with a bare silicon wafer to control the thickness of the PDMS membrane to 500 μm. The assembly was then cured at 80 °C for 5 h. (e) The top wafer was removed carefully and the cured PDMS membrane was cut to 20 mm × 20 mm and peeled off the master.

(B) Microfabriated SU-8 master for the lid. (*top*) Photo of the surface and (*bottom*) surface scan with a contact stylus profiler (KLA-Tencor P-16+) along the red dashed line in the (top) image. The patterns contained squares (a) 150 μm on a 200 μm grid or (b) 300 μm on a 400 μm grid; or rectangles (c) 500 μm × 150 μm on a 600 μm × 200 μm grid, and (d) 1000 μm × 300 μm on a 1200 μm × 400 μm grid. The size and spacing of the posts was not critical; for each device an array of posts was selected with dimensions that facilitated sealing of complete arrays of dimples. The height of the posts was 28 μm in all structures.

Figure S3. Lid-dimple assembly

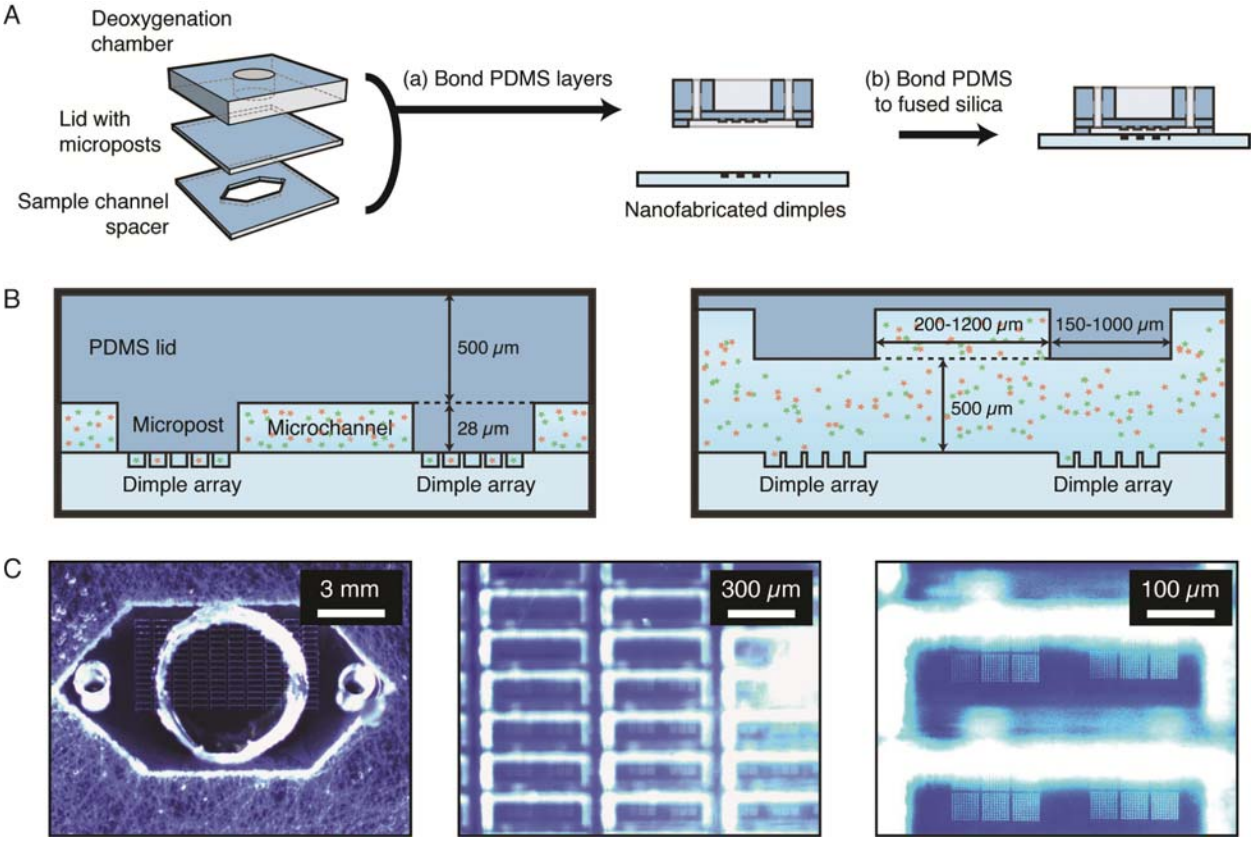

(A) Scheme for the lid-dimple assembly. (a) Three layers of PDMS were prepared: (1) a deoxygenation chamber with ϕ = 5 mm hole in a slab (3-mm-thick), (2) the microfabricated lid membrane with microposts (500-μm-thick) (Figure S2), and (3) a spacer with a hexagonal sample channel cut out with a knife (500-μm-thick). Surfaces of these layers were activated by oxygen plasma for 1 min (SPI, Plasma-Prep II) and then irreversibly bonded. (b) Two ports for sample injection were punched into the PDMS lid complex using a blunt needle (18G). The microposts on the lid were aligned to the dimple arrays by assembly under a dissecting microscope with a custom three-axis aligner (Thorlabs, DT12). The reversible bonding between PDMS and fused silica was strong enough to remain stable throughout the experiment and allowed disassembly, cleaning, and reuse without sacrificing the lid or the substrate.

(B) Cartoon of the sample channel. The lid is shown when (*left*) sealing and (*right*) refreshing the dimples.

(C) Microscope images of the PDMS lid assembly. (*left*) A full view of the sample channel from the top. (*middle*) Micropost arrays placed on the dimple substrate. (*right*) A close view of the dimple arrays aligned under the rectangular microposts.

Part II. Methods for the Dimple Machine

Section S1. Experimental setup and procedures

Optical setup. An alternating laser excitation (ALEX) setup equipped with a dual-view EM-CCD (Andor iXon, DU-897E-CS0-#BV, 512 × 512 with 16 μm pixels) was constructed (Figure 1) by adapting protocols described elsewhere.[S1,S2] Briefly, two laser beams (638 and 532 nm) were combined using a dichroic mirror, and the intensity of each was modulated by an acousto-optical tunable filter (Gooch & Housego, PCAOM 48058-2.5-.55-5W). The microscope contained a dual-band excitation filter (Chroma, z532/635rpc). The molecules were illuminated in epifluorescence mode with a 60 X oil-immersion objective (Olympus, 1-U2B616, N.A. 1.45) mounted on an inverted epifluorescence microscope (Olympus, IX71). Typical illumination intensities were 100 W/cm^2. The fluorescence image exiting the microscope was cropped to half with a slit, and then separated into two channels (red and green) by a dichroic mirror. Each channel was imaged on one half of the CCD detector.

Sample preparation. Three sets of fluorescently labeled single-stranded DNA (ssDNA) oligos were purchased from IDT: a non-complementary pair, a doubly labeled hairpin, and a hybridizing pair (Table S3).

Preparation for trapping. Prior to trapping, the sample channel was incubated with 1 % polyvinylpyrrolidone (PVP, Sigma-Aldrich) for 2 h to minimize adsorption of molecules on the fused silica. The sample channel was then washed with 0.1 % PVP multiple times, and briefly degassed in a desiccator. The experimental sample (40 μL) was then injected into the sample channel. All trapping experiments were carried out in the "trapping buffer" containing 25 mM HEPES at pH 8.0 with 150 mM sodium chloride and with low concentrations of additives to minimize surface effect and improve photostability (Table S1). The deoxygenation reservoir on the top of the PDMS lid was filled with 200 μL of deoxygenation buffer (Table S2) to further deoxygenate the sample (Figure S4). Polyethylene tubing (BD, PE-90) was inserted into the ports of sample channel, and connected to house vacuum via a solenoid valve (Warner, VC-8). The device was placed on a microscope stage and then enclosed in a plastic box containing wet towels to maintain humidity. The box was purged with a constant flow (< 2 scfh) of humidified nitrogen throughout the measurement.

Trapping and measurement. The scheme for pneumatically actuating the PDMS lid (Figure 1) was adapted from Ref. S3. Briefly, the lid was actuated by applying vacuum to both ports of the sample chamber. Atmospheric pressure on the top of the lid then caused the lid to bow down until it contacted the silica coverslip, sealing the dimples.

We found that it was typically necessary to wait ~5 min between actuation of the vacuum and imaging for the lid to achieve a hermetic seal with the fused silica. Each cycle consisted of 90 s of data acquisition at an exposure time of 50 ms/frame. Red and green laser excitations were applied on alternate frames. The EM-CCD gain was 300. To refresh the dimples, the vacuum was released and the lid returned to its raised position. The lid actuation, alternating laser excitation, and camera exposures were synchronized by a Data Acquisition board (National Instruments, PCIe-6323) run by custom software (LabView, National Instruments).

Device storage. After experiments the Dimple Machine was washed by flowing 0.1 % PVP and 0.1 % Tween-20 (Sigma-Aldrich) through the sample channel. The washed device was stored in 4 °C with 0.1 % PVP and 0.02 % sodium azide in the sample channel to inhibit the growth of bacteria. It was not necessary to condition the device with 1 % PVP again for the next experiment. If needed, the dimple array substrate was detached from the PDMS lid, cleaned in piranha solution, and bonded to the lid again.

Data analysis. Data was analyzed with custom software written in MATLAB (R2011a, MathWorks). Briefly, three sets of fluorescence time traces were extracted: (a) $D(t)$: green emission under green excitation; (b) $A(t)$: red emission under green excitation; and (c) $R(t)$: red emission under red excitation. The fluorescence intensity from each dimple was extracted from the 7×7 pixels (typical) centered on the dimple, and the background fluorescence estimated from neighboring pixels was subtracted from the dimple intensity. To estimate the occupancy by red molecules, we looked at $R(t)$; to estimate the occupancy by green molecules, we looked at $G(t) = D(t) + A(t)$. The occupancy was measured by counting the number of fluorescent dyes as described in Figure S5. A 2D histogram of red and green fluorescence (R-G histogram) was constructed in a similar way to Figure S5, but with two traces $R(t)$ and $G(t)$. When analyzing FRET, a 2D histogram of acceptor and donor fluorescence (A-D histogram) was constructed similarly using $D(t)$ and $A(t)$. Data traces in which we observed a photobleaching event were excluded from kinetic or thermodynamic analysis.[S1]

Section S2. Optimization

Background autofluorescence from fused silica. Minimizing background fluorescence in single-molecule measurements is crucial to enhance signal-to-noise ratio. Fused silica shows very low autofluorescence. However, we observed a high level of autofluorescence (especially under red excitation) in the regions of the sample exposed to the electron beam during electron-beam lithography. While this phenomenon was documented previously,[S4] we did not find any remedies in the literature. We discovered that by baking the substrate in furnace at 900 °C for 5 h the autofluorescence decreased to the initial low level.

Reproducibility of trapping. To achieve reproducible trapping, we found that it was necessary to lower the PDMS lid at the same rate, and with the same force, every time. To achieve this reproducibility, actuation of the lid was controlled by a digital vacuum valve with precise timing to open and close (Section S1). This feature ensured reproducible repetition of the trapping, producing a large dataset without artifact (Figure S6).

Nonspecific adsorption of molecules on the fused silica and PDMS surface. Biomolecules such as DNA and proteins adsorb onto many surfaces, especially on hydrophobic ones. This nonspecific sticking creates background fluorescence that interferes with observations of single molecules. Polyvinylpyrrolidone (PVP) generates a physically adsorbed barrier that prevents nonspecific adsorption of DNA on the fused silica and PDMS.[S6,S7] Incubation with PVP solution for 2 h prior to the first experiment, suppressed sticking of DNA oligos on fused silica surface effectively. We also mixed the sample with PVP (0.1%) and Tween-20 (0.1%) to minimize sticking of molecules on the fused silica and PDMS surface, respectively (Figure S6C).

Suppression of photobleaching. Photobleaching can be suppressed by enzymatic deoxygenation of the solution. We first used protocatechuic acid (PCA) / protocatechuate-3,4-dioxygenase (PCD) to deoxygenate the sample enzymatically.[S5] However, this approach was not effective because (1) The PCD enzyme was typically at a concentration so low that many dimples contained zero PCD molecules; and (2) Oxygen has high solubility in and permeability through PDMS, so the PDMS lid acted as a large reservoir of oxygen, easily overwhelming the capacity of the oxygen scavengers in the dimples. We improved deoxygenation by combining three approaches (Figure S4A).

(1) *Enzymatic oxygen scavenging in the microchannels*. We designed a PDMS lid with microposts. When the lid was closed, the inverted posts on the lid sealed the dimple array, creating microchannels around the array. The

channels then irrigated bulk solution near to the dimple array (~ 100 μm), providing a large sink for oxygen close to the dimples.

(2) *Remote deoxygenation from across the lid membrane*. We exploited the oxygen permeability of PDMS to de-oxygenate the dimples from the top side of the PDMS lid. The reservoir on top of the PDMS lid was loaded with deoxygenation buffer (Table S2). This reservoir generated a reversed oxygen concentration gradient spanning the lid membrane, causing oxygen to diffuse *out* of the dimples and into the PDMS lid.

(3) *Operation in a nitrogen atmosphere.* A constant flow of house N_2 was blown into a humidified box covering the device. This physical exclusion of oxygen from the sample chamber prolonged the lifetime of the oxygen scavenger reservoir, facilitating long-term measurements.

In addition to PCA/PCD, we added methyl viologen (1 mM) and ascorbic acid (1 mM) as a redox system quenching the triplet states of fluorescent dyes, and thereby suppressing photoblinking.[S8]

Leakage of molecules out of the dimples. Reliable sealing of the dimples is a prerequisite of trapping and accurate measurement of occupancy. The surface roughness of the substrate must be smaller than the length-scale of the molecules to be trapped, typically ~1 nm. Clean fused silica has surface roughness below 1 nm (Figure S1B). However, plasma etching or exposure to extremes of pH gradually roughened the surface, necessitating care in cleaning. A thin aqueous film often persisted between the fused silica and the lid immediately after closing the lid. This film permitted molecules to escape from the dimples. To facilitate the draining of this film, we introduced the post topography into the PDMS lid, thereby minimizing the distance the water had to flow to reach a deep channel. After introducing the posts, we found that the lid sealed hermetically after ~5 min.

Diffusion of water into the PDMS lid leading to drying of the dimples. PDMS absorbs water to a small extent. Each sealed dimple contained < 1 fL of water, which easily was absorbed into the PDMS lid. The deoxygenation buffer on top of the lid also saturated the lid with water, preventing additional absorption of water from the dimples. The device was run inside a humidified chamber to prevent drying of the deoxygenation buffer. The sealed dimples remained hydrated until the deoxygenation buffer completely dried out, usually after more than 1 day.

Avoidance of air bubbles in the sample channel. Application of vacuum to the sample channel induced formation of micro-bubbles in the channel. To avoid bubbles, (1) the sample solution was injected with a micropipette with minimal speed of loading, and (2) the device was degassed for a few minutes in a vacuum desiccator prior to use.

Table S1. Composition of the trapping buffer

Material	Concentration	Role
HEPES	25 mM	Buffer at pH 8.0
NaCl	150 mM	Ionic strength
Polyvinylpyrrolidone (Avg. MW 10 kDa)	0.1 %	Prevents sticking on fused silica
Tween 20	0.1 %	Prevents sticking on PDMS
Methyl viologen dichloride	1 mM	Triplet-state quencher (oxidant)
Sodium L-ascorbate	1 mM	Triplet-state quencher (reductant)
Protocatechuic acid	10 mM	Enzymatic deoxygenation (substrate)
Protocatechuate 3,4-dioxygenase	0.1 μM	Enzymatic deoxygenation (enzyme)

* All materials in Table S1 and S2 were purchased from Sigma-Aldrich.

Table S2. Composition of the deoxygenation buffer

Material	Concentration	Role
HEPES	25 mM	Buffer at pH 8.0
Tween 20	0.1 %	Prevents sticking on PDMS
Protocatechuic acid	10 mM	Enzymatic deoxygenation (substrate)
Protocatechuate 3,4-dioxygenase	0.1 μM	Enzymatic deoxygenation (enzyme)

* All materials in Table S1 and S2 were purchased from Sigma-Aldrich.

Part III. Verification of the Dimple Machine

Figure S4. Suppression of photobleaching

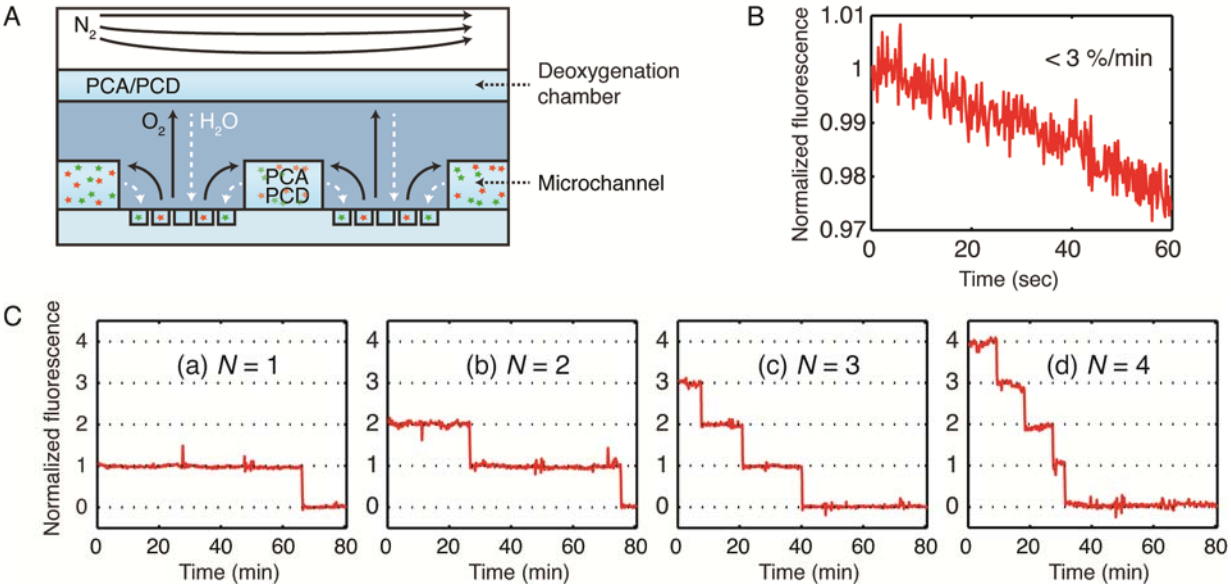

(A) Scheme for the suppression of photobleaching. The dimples were deoxygenated by three methods: (1) Enzymatic oxygen scavenging in the microchannels; (2) Remote deoxygenation from across the lid membrane; and (3) Nitrogen atmosphere surrounding the device (Section S2). Note that water molecules can also diffuse through PDMS, indicated by the white dashed arrows (Section S2).

(B) Decay of fluorescence due to photobleaching. The fluorescence is averaged over 100 dimples and 60 cycles. Less than 3 % of fluorescence photobleached in 1 min.

(C) Prolonged observation of single molecules. Fluorescence intensity traces showing single-step photobleaching for (a) 1, (b) 2, (c) 3, and (d) 4 fluorescent dyes in a single dimple. In these experiments the lid was kept sealed throughout.

Figure S5. Counting of fluorescent dyes in a dimple

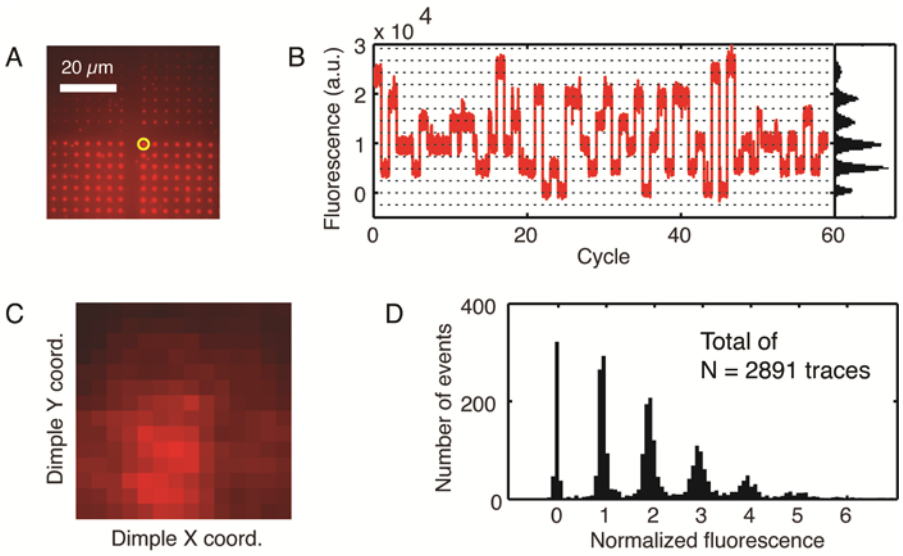

(A) Fluorescence image of a dimple array averaged over time. The yellow circle marks the dimple whose time trace is plotted in (B).

(B) Fluorescence time trace of a dimple. The data is concatenated over 60 trapping cycles. Cycles lasted 1 min and were spaced by 5 min. The intensity histogram of the trace is attached on the right. The unit fluorescence intensity from a single dye was obtained from the average spacing of peaks in the histogram.

(C) A map unit fluorescence of a dimple array. The intensity of each pixel represents the unit fluorescence for each dimple shown in (A). The total fluorescence from each dimple was normalized by the corresponding unit fluorescence to measure occupancy.

(D) Histogram of normalized fluorescence. The graph is for 2891 time traces recorded from across the array.

Figure S6. Reproducible filling of dimples

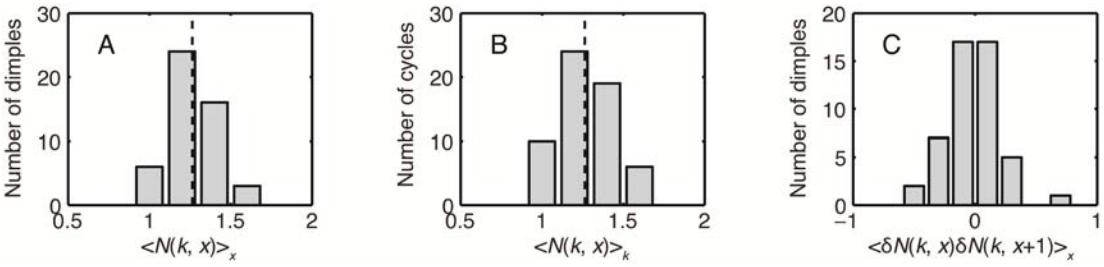

The quantity $N(k, x)$ represents the occupancy of the k-th dimple in the x-th cycle of trapping.

(A) The occupancy distribution for individual dimples averaged over cycles. The dashed line indicates the average occupancy over all dimples. This distribution shows that there were not significant variations in dimple volume.

(B) The occupancy distribution for individual cycles averaged over dimples. The dashed line indicates the average occupancy over all cycles. This distribution shows that there were not significant variations in mean dimple occupancy from cycle to cycle.

(C) Correlation in the single-dimple occupancy over consecutive cycles. The distribution of correlations (for 60 cycles) is centered on zero, indicating that the loading of the dimples was uncorrelated between successive cycles. This result confirms complete interchange of dimple contents during each refresh cycle.

Part IV. Measurement of interaction using red-green correlation

Table S3. DNA sequences

Linkage	Sequence	Length (bp)
None	R: 5'-/Cy5/-TCT AGT CTC CCC AAA AAA AAA AAA AAA AAA-3'	30
	G: 5'-ATG TCT GAC GCT GGC ATT CGC ATC AAA GGA-/Cy3/-3'	30
Covalent	RG: 5'-GCA ATT TAT TAA TTA TAT ATT TTA TTT AAT ATA ATT/Alexa647/ CCT GGA TCC GCA AGC TGG CGT TTA GTG ATA TCC CGT ATA AGT CTG TAG TGA ATT CTC C/Cy3B/TA TTA TAT TAA ATA AAA TAT ATA ATT AAT AAA TTG C-3'	130
Hybridization	R: 5'-/Cy5/-TCT AGT CTC CCC AAA AAA AAA AAA AAA AAA-3'	30
	G: 5'-/Cy3/-AGA CTA GAC CCC AAA AAA AAA AAA AAA AAA-3'	30

* All DNA samples were ordered form IDT. The ssDNA oligo "R" of the hybridization pair was used in the proof-of-principle occupancy measurement in Figure 2 and Figure S4–S6.

Figure S7. Measurement of K_d from correlated occupancy

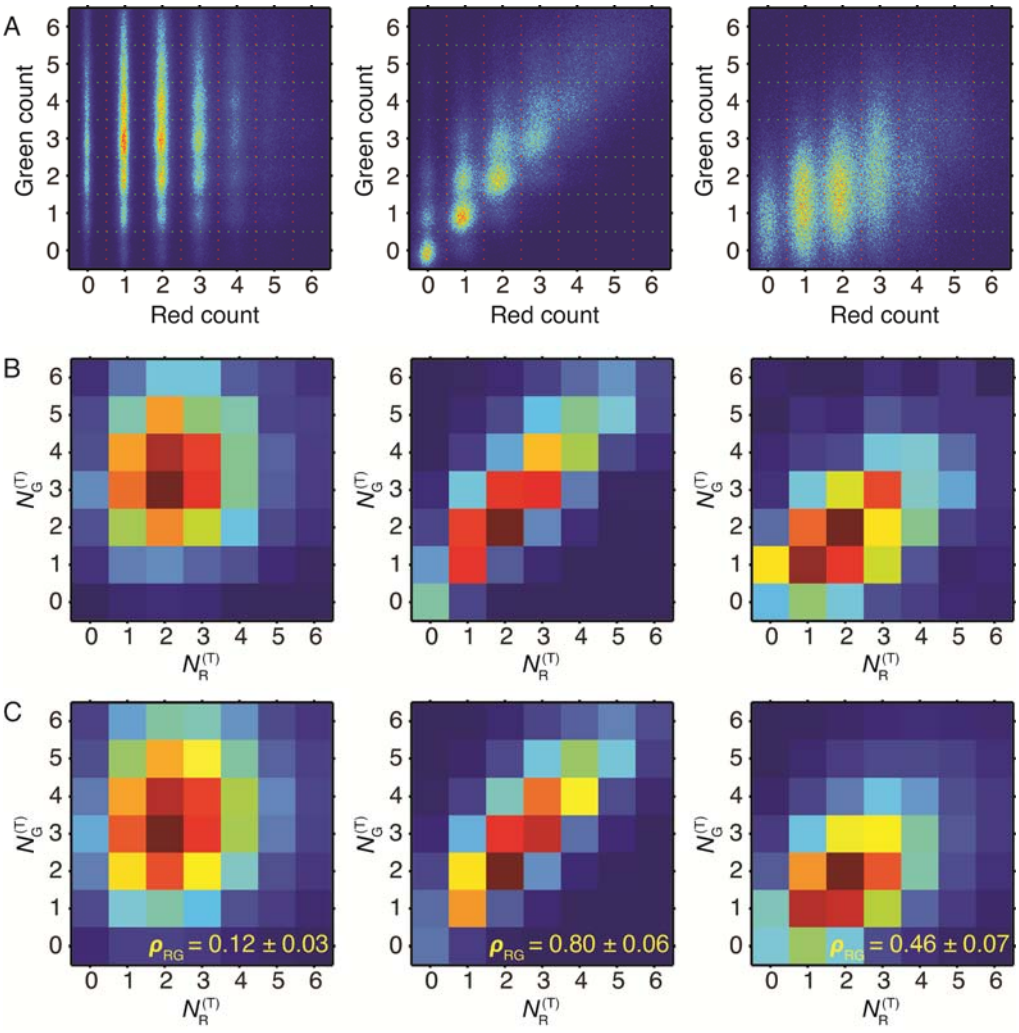

(*left*) Non-complementary, (*center*) covalently linked, and (*right*) hybridizing ssDNA pairs.

(A) R-G histogram of the unfiltered raw fluorescence. The R-G histograms shown in the main text were obtained from the raw fluorescence traces by application of a median filter running over 13 frames.

(B) R-G histogram of the rounded fluorescence. The mean normalized fluorescence from each dimple in each cycle was rounded to the nearest integer value, to provide an estimate of occupancy.

(C) Correlated bivariate Poisson fit to the R-G histograms in (B). Fitting parameters are given in Table S4.

Table S4. Fitting parameters for a correlated bivariate Poisson model

Linkage	None	Covalent	Hybridization
λ_R	2.21 ± 0.11	0.31 ± 0.04	1.39 ± 0.13
λ_G	3.43 ± 0.12	0.96 ± 0.05	1.09 ± 0.14
λ_{RG}	0.39 ± 0.10	2.50 ± 0.07	1.07 ± 0.13
ρ_{RG}	0.12 ± 0.03	0.80 ± 0.06	0.46 ± 0.07
K_d (nM)	900 ± 200	1.10 ± 0.15	63 ± 12

* The dimple occupancy by two spectrally distinguishable interacting species (R and G in the main text) was modeled as a correlated bivariate Poisson distribution (Section S3).

Section S3. Theory of correlated bivariate Poisson distribution

When a mixture of R, G, and RG is trapped in dimples, each species assorts independently, following its own Poisson distribution:

$$f_{\mathrm{R}}(N)=\frac{(\lambda_{\mathrm{R}})^{N}e^{-\lambda_{\mathrm{R}}}}{N!},\ f_{\mathrm{G}}(N)=\frac{(\lambda_{\mathrm{G}})^{N}e^{-\lambda_{\mathrm{G}}}}{N!},\text{ and }f_{\mathrm{RG}}(N)=\frac{(\lambda_{\mathrm{RG}})^{N}e^{-\lambda_{\mathrm{RG}}}}{N!} \tag{1}$$

where λ_{R}, λ_{G}, and λ_{RG} are the average occupancy of dimples by R, G, and RG, respectively. Consider a dimple with a joint occupancy, $(N_{\mathrm{R}}^{(\mathrm{T})},N_{\mathrm{G}}^{(\mathrm{T})})$. If there are N_{RG} molecules of RG in this dimple, the occupancy by monomeric R and G are $N_{\mathrm{R}}=N_{\mathrm{R}}^{(\mathrm{T})}-N_{\mathrm{RG}}$ and $N_{\mathrm{G}}=N_{\mathrm{G}}^{(\mathrm{T})}-N_{\mathrm{RG}}$, respectively. The probability of the joint distribution is

$$\mathrm{P}(N_{\mathrm{R}}^{(\mathrm{T})},N_{\mathrm{G}}^{(\mathrm{T})})=\sum_{N_{\mathrm{RG}}=0}^{N_{\mathrm{RG}}^{\max}}f_{\mathrm{R}}(N_{\mathrm{R}}^{(\mathrm{T})}-N_{\mathrm{RG}})f_{\mathrm{G}}(N_{\mathrm{G}}^{(\mathrm{T})}-N_{\mathrm{RG}})f_{\mathrm{RG}}(N_{\mathrm{RG}}) \tag{2}$$

Plugging in Eq. 1 into Eq. 2 results in the following expression:

$$\mathrm{P}(N_{\mathrm{R}}^{(\mathrm{T})},N_{\mathrm{G}}^{(\mathrm{T})})=e^{-(\lambda_{\mathrm{R}}+\lambda_{\mathrm{G}}+\lambda_{\mathrm{RG}})}(\lambda_{\mathrm{R}})^{N_{\mathrm{R}}^{(\mathrm{T})}}(\lambda_{\mathrm{G}})^{N_{\mathrm{G}}^{(\mathrm{T})}}\left(-\frac{\lambda_{\mathrm{R}}\lambda_{\mathrm{G}}}{\lambda_{\mathrm{RG}}}\right)^{-N_{\mathrm{G}}^{(\mathrm{T})}}U\left(-N_{\mathrm{G}}^{(\mathrm{T})},1-N_{\mathrm{G}}^{(\mathrm{T})}+N_{\mathrm{R}}^{(\mathrm{T})},-\frac{\lambda_{\mathrm{R}}\lambda_{\mathrm{G}}}{\lambda_{\mathrm{RG}}}\right) \tag{3}$$

where U represents the Tricomi confluent hypergeometric function:

$$U(a,b,z)=\frac{1}{\Gamma(a)}\int_{0}^{\infty}e^{-zt}t^{a-1}(1+t)^{b-a-1}dt\,. \tag{4}$$

Eq. 3 serves as a model for the joint distribution with three fitting parameters λ_{R}, λ_{G}, and λ_{RG}. After fitting the experimental R-G histogram to Eq. 3, the correlation coefficient ρ_{RG} between R and G is obtained by

$$\rho_{\mathrm{RG}}=\frac{\lambda_{\mathrm{RG}}}{\sqrt{(\lambda_{\mathrm{R}}+\lambda_{\mathrm{RG}})(\lambda_{\mathrm{G}}+\lambda_{\mathrm{RG}})}}. \tag{5}$$

One can infer the equilibrium concentration of species in bulk from the average occupancy of dimples (Figure S7, Table S4). The dissociation constant is:

$$K_{\mathrm{d}}=\frac{[\mathrm{R}]_{\mathrm{eq}}[\mathrm{G}]_{\mathrm{eq}}}{[\mathrm{RG}]_{\mathrm{eq}}}=\frac{(\lambda_{\mathrm{R}}/(N_{\mathrm{A}}V_{\mathrm{d}}))(\lambda_{\mathrm{G}}/(N_{\mathrm{A}}V_{\mathrm{d}}))}{\lambda_{\mathrm{RG}}/(N_{\mathrm{A}}V_{\mathrm{d}})}. \tag{6}$$

Part V. DNA hybridization in dimples

Section S4. Bulk measurement of K_d

Experimental procedure. Equimolar mixtures of two hybridizing ssDNA oligos (Table S3) were prepared at various concentrations from 2 nM to 2 μM in HEPES buffer at pH 8.0 with 150 mM NaCl. The fluorescence emission spectra of the mixture were measured in a fluorimeter (Cary Eclipse, Agilent) exciting the sample at 550 nm, collecting the emission from 550 nm to 750 nm (Figure S8A). The emission intensity at 670 nm was selected as a value representing the intensity of FRET acceptor emission and plotted against concentrations (Figure S8B).

Analysis: Fraction of dimer in a binary mixture. When R and G associate in a mixture, they exist in equilibrium with the bound form, RG:

$$\mathrm{R} + \mathrm{G} \rightleftarrows \mathrm{RG} \tag{1}$$

with the relative fraction of each species determined by the dissociation constant K_d:

$$K_d = \frac{[\mathrm{R}]_{eq}[\mathrm{G}]_{eq}}{[\mathrm{RG}]_{eq}} = \frac{([\mathrm{R}]_0 - [\mathrm{RG}]_{eq})([\mathrm{G}]_0 - [\mathrm{RG}]_{eq})}{[\mathrm{RG}]_{eq}} \tag{2}$$

where $[R]_{eq}$, $[G]_{eq}$, and $[RG]_{eq}$ are the equilibrium concentrations of R, G, and RG, respectively, and $[R]_0$ and $[G]_0$ are the initial concentrations of R and G, respectively. Solving Eq. 2 for $[RG]_{eq}$ as a function of $[R]_0$, $[G]_0$, and K_d gives

$$[\mathrm{RG}]_{eq} = \frac{1}{2}\left([\mathrm{R}]_0 + [\mathrm{G}]_0 + K_d - \sqrt{([\mathrm{R}]_0 + [\mathrm{G}]_0 + K_d)^2 - 4[\mathrm{R}]_0[\mathrm{G}]_0}\right). \tag{3}$$

In our study, the FRET efficiency is low when R is unbound, and high when bound to G. If the acceptor emission intensity is I_{low} in R and I_{high} in RG, the average acceptor intensity I_A is

$$\langle I_A \rangle = \left(\frac{[\mathrm{R}]_{eq}}{[\mathrm{R}]_0}\right) I_{low} + \left(\frac{[\mathrm{RG}]_{eq}}{[\mathrm{R}]_0}\right) I_{high} = I_{low} + \left(\frac{[\mathrm{RG}]_{eq}}{[\mathrm{R}]_0}\right)(I_{high} - I_{low}) \tag{4}$$

Substituting Eq. 3 into Eq. 4 gives a model for the acceptor emission. This model was fit to the experimental curve to obtain K_d (Figure S8B).

Figure S8. Bulk measurement of K_d

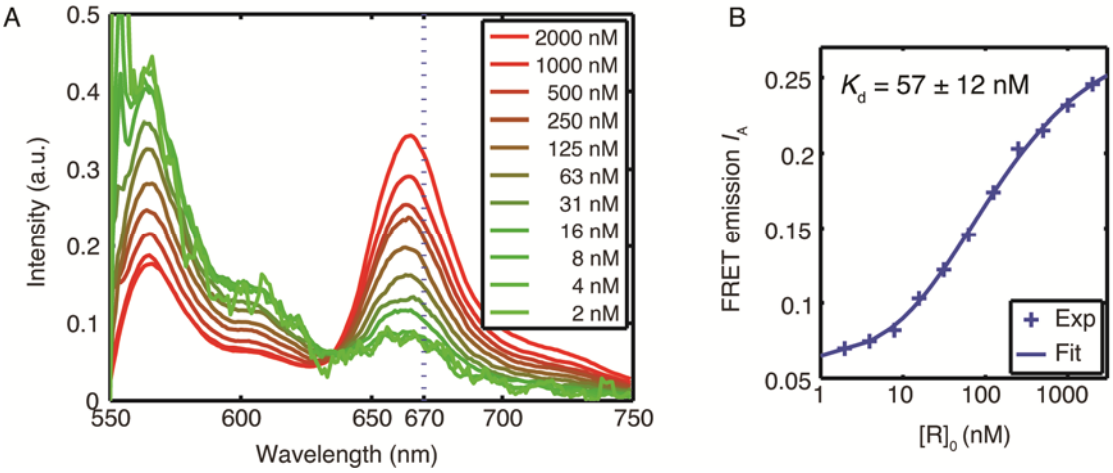

See Section S4 for the methods of experiment and analysis.

(A) Fluorescence emission spectra of the hybridizing ssDNA pair mixtures. The spectra are measured in a fluorospectrometer at the excitation wavelength of 550 nm at various initial concentrations (legend). The dashed line (emission at 670 nm) indicates the wavelength at which the FRET acceptor emission is taken.

(B) FRET acceptor emission intensity as a function of initial concentration of DNA, $[R]_0$. The K_d extracted from the curve was 57 ± 12 nM. Exp: Experimental data; Fit: Fitted curve.

Section S5. Theory of multi-state Markov process

Steady-state distributions

Consider a dimple with a joint occupancy $(N_{\mathrm{R}}^{(\mathrm{T})}, N_{\mathrm{G}}^{(\mathrm{T})})$ in which R and G associate and dissociate with rate constants k_{on} and k_{off}, respectively. Assuming that the reaction is Markovian, the number of dimers at time t, $N_{\mathrm{RG}}(t)$ can be considered as a state variable whose path is determined by the kinetic matrix **M** with the element m_{ij} representing the transition rate from state j to state i:

$$m_{ij} = \lim_{\Delta t \to 0} \frac{\mathrm{P}[N_{\mathrm{RG}}(t+\Delta t) = i \,|\, N_{\mathrm{RG}}(t) = j] - \delta_{ij}}{\Delta t} \quad (i, j = 0,1,\cdots, N_{\mathrm{RG}}^{\max}) \tag{1}$$

where $N_{\mathrm{RG}}^{\max}$ is the maximum number of RG given by $\min(N_{\mathrm{R}}^{(\mathrm{T})}, N_{\mathrm{G}}^{(\mathrm{T})})$. Note that to avoid confusion, the matrix indices i and j start from zero. Only certain elements of the rate matrix are non-zero. These are:

$$m_{(i+1)i} = k_{\mathrm{on}}[\mathrm{R}][\mathrm{G}] = k_{\mathrm{on}} \frac{N_{\mathrm{R}}}{N_{\mathrm{A}} V_{\mathrm{d}}} \frac{N_{\mathrm{G}}}{N_{\mathrm{A}} V_{\mathrm{d}}}$$

$$= k_{\mathrm{on}} \frac{(N_{\mathrm{R}}^{(\mathrm{T})} - i)}{N_{\mathrm{A}} V_{\mathrm{d}}} \frac{(N_{\mathrm{G}}^{(\mathrm{T})} - i)}{N_{\mathrm{A}} V_{\mathrm{d}}}, \quad (i = 0,1,\cdots, N_{\mathrm{RG}}^{\max} - 1) \tag{2}$$

$$m_{i(i+1)} = k_{\mathrm{off}}[\mathrm{RG}] = k_{\mathrm{off}} \frac{N_{\mathrm{RG}}}{N_{\mathrm{A}} V_{\mathrm{d}}}$$

$$= k_{\mathrm{off}} \frac{i+1}{N_{\mathrm{A}} V_{\mathrm{d}}}, \quad (i = 0,1,\cdots, N_{\mathrm{RG}}^{\max} - 1) \tag{3}$$

$$m_{ii} = -\sum_{j \neq i} m_{ji} = -m_{(i+1)i} - m_{(i-1)i}, \tag{4}$$

where N_{A} is Avogadro's number, and V_{d} is the volume of the dimple. All other elements of **M** are zero.

To calculate the steady state probability distribution, we apply the condition of detailed balance between state j and j+1:

$$m_{j(j+1)} \mathrm{P}_{j+1} = m_{(j+1)j} \mathrm{P}_j. \tag{5}$$

Applying this condition recursively from P_0 yields:

$$\mathrm{P}_i = \left(\prod_{j=0}^{i-1} \frac{m_{(j+1)j}}{m_{j(j+1)}} \right) \cdot \mathrm{P}_0. \quad (i = 1,2,\cdots, N_{\mathrm{RG}}^{\max}) \tag{6}$$

Substituting Eqs. 2 and 3 into Eq. 6 gives an expression for the steady-state distributions relative to P_0:

$$P_i = \frac{N_R^{(T)}! N_G^{(T)}!}{i!(N_R^{(T)} - i)!(N_G^{(T)} - i)!}\left(\frac{k_{on}}{N_A V_d \cdot k_{off}}\right)^i P_0 . \quad (7)$$

Applying the condition $\sum P_i = 1$ yields:

$$\overline{P}_i = \frac{P_i}{\sum_j P_j} . \quad (8)$$

Eq. 10 can also be derived from equilibrium statistical mechanics as $\frac{P_i}{P_0} = \frac{g_i}{g_0}\exp(-i\Delta G / k_B T)$, where g_i is the degeneracy of state i and $i\Delta G$ is the free energy to form i molecules of product.

An important feature of Eq. 7 is that the steady-state distribution of dimer depends not only on the reaction equilibrium ($K_d = k_{off}/k_{on}$), but also on the dimple volume and on the stochastically determined occupancy.

Autocorrelations

The second-order autocorrelation, $C^{(2)}(\tau)$ of the state variable $i = N_{RG}(t)$ is predicted by summing the conditional probabilities of $N_{RG}(t)$ for the two time points separated by τ:

$$C^{(2)}(\tau) = \left(\sum_{j=0}^{N_{RG}^{max}} j P[N_{RG}(\tau) = j | N_{RG}(0) = i]\right)\left(\sum_{i=0}^{N_{RG}^{max}} i P[N_{RG}(0) = i]\right) - \langle N_{RG} \rangle^2 \quad (9)$$

$$= \mathbf{1N}e^{\mathbf{M}\tau}\mathbf{NP}_{eq} - (\mathbf{1NP}_{eq})^2 \quad (10)$$

where $\mathbf{N}$ is a $(N_{RG}^{max}+1)\times(N_{RG}^{max}+1)$ diagonal matrix with $\mathbf{N}_{ii} = i$, and $\mathbf{1}$ is a row vector of ones.[S9]

For the $(N_R^{(T)}, N_G^{(T)})$ pairs with $N_{RG}^{max} = 1$ (i.e., two-state process), Eq. 10 reduces to a simple formula

$$C^{(2)}(\tau) = \frac{r_{on} r_{off}}{(r_{on} + r_{off})^2} e^{-(r_{on}+r_{off})\tau} \quad (11)$$

where r_{on} and r_{off} are the on- and off-rates of the reaction, respectively. Eq. 2 and 3 gives

$$r_{on} = \frac{k_{on} N_R^{(T)} N_G^{(T)}}{(N_A V_d)} \text{ and } r_{off} = k_{off} . \quad (12)$$

The condition $N_{\mathrm{RG}}^{\max} = 1$ implies that at least one of $N_{\mathrm{R}}^{(\mathrm{T})}$ or $N_{\mathrm{G}}^{(\mathrm{T})}$ equals 1; however one of these quantities can be greater than 1. The quantity $N_{\mathrm{RG}}(t)$ was proportional to the acceptor fluorescence, so we calculated the autocorrelation $C_{AA}^{(2)}(\tau)$:

$$C_{AA}^{(2)}(\tau) = \left\langle \delta A(t+\tau)\, \delta A(t) \right\rangle \tag{13}$$

where δ represents the difference from the average. The autocorrelation was then fit to a model (Eq. 11) to extract k_{on} and k_{off} (Figure 6b).

We calculated the autocorrelations for higher occupancies numerically by Eq. 9, keeping the k_{on} and k_{off} estimates from the two-state autocorrelations. The calculated curves agreed well to the measurement for all high-occupancy correlations, confirming that the rate constants are not dependent on occupancy.

References

S1. Kapanidis, A. N.; Laurence, T. A.; Lee, N. K.; Margeat, E.; Kong, X.; Weiss, S. *Acc. Chem. Res.* **2005**, *38*, 523–533.

S2. Roy, R.; Hohng, S.; Ha, T. *Nat. Meth.* **2008**, *5*, 507–516.

S3. Sims, P. A.; Greenleaf, W. J.; Duan, H.; Xie, X. S. *Nat. Meth.* **2011**, *8*, 575–580.

S4. Peters, H.; Schultes, R. *Phys. Rev.* **1930**, *36*, 1631–1635.

S5. Aitken, C. E.; Marshall, R. A.; Puglisi, J. D. *Biophys. J.* **2008**, *94*, 1826–1835.

S6. Dorfman, K. D. *Rev. Mod. Phys.* **2010**, *82*, 2903–2947.

S7. Xia, Y.-M.; Hua, Z.-S.; Srivannavit, O.; Ozel, A. B.; Gulari, E. *J. Chem. Technol. Biotechnol.* **2007**, *82*, 33–38.

S8. Vogelsang, J.; Kasper, R.; Steinhauer, C.; Person, B.; Heilemann, M.; Sauer, M.; Tinnefeld, P. *Angew. Chem., Int. Ed.* **2008**, *47*, 5465–5469.

S9. Fredkin, D. R.; Rice, J. A. *Math. Biosci.* **1987**, *87*, 161–172.